Investigating the Linkage Between Spiral Trough Morphology and Cloud Coverage on the Martian North Polar Layered Deposits

K. A. Lutz[1], R. L. Hawley[1], and M. C. Palucis[1]

[1]Department of Earth Sciences, Dartmouth College, Hanover, NH, United States

Corresponding author: Katherine Lutz (katherine.a.lutz.gr@dartmouth.edu)

Key Points:

- The spiral troughs on Mars' northern polar layered deposits (NPLD) have highly variable geometry, both within a trough and between troughs.
- The presence of trough-parallel clouds, indicative of katabatic jumps and active trough migration, are regionally variable across the NPLD.
- Trough shape most conducive to the formation of katabatic jumps and generating clouds is not as widespread as previously suggested.

Abstract

The Martian North Polar Layered Deposits (NPLD) are composed of alternating water-ice and dust-rich layers resulting from atmospheric deposition and are key to understanding Mars' climate cycles. Within these deposits are spiral troughs, whose migration affects deposition signals. To understand the relationship between NPLD stratigraphy and Martian climate, we must identify modern-day drivers of NPLD ice migration. Prevailing theory posits migration driven by upstream-migrating bed undulations bounded by hydraulic jumps, caused by katabatic winds flowing over trough walls with asymmetric cross-sectional relief. This is supported by trough-parallel clouds, whose formation has been attributed to hydraulic jumps. We present a cloud atlas across the Martian north pole using ~13,800 THEMIS images spanning ~18 Earth years. We find trough-parallel clouds in ~400 images, with regions nearer to the pole having higher cloud frequency. We compare spiral trough geometry to our cloud atlas and find regions with trough-parallel clouds often correlate with metrics associated with modern-day sublimation-deposition cycles (i.e., relief and asymmetry), but not always. In some regions, troughs with morphologies conducive to cloud formation have no clouds. Overall, trough geometry varies greatly across the deposits, both within and between troughs, suggesting localized differences in deposition relative to migration, varying katabatic wind intensities, differing past climatic states influencing the troughs, varying trough initiation properties, or the possibility of additional mechanisms for trough initiation and migration (e.g., in-situ trough erosion). Understanding what controls trough shape variability across the NPLD and how these controls change through time and space is key when interpreting Martian paleoclimate.

Plain Language Summary

The Martian North polar ice cap is composed of layers of water-ice and dust deposited from the atmosphere, and differences in their thicknesses are thought to be the result of climate variations. Interpretations of the climate recorded in these layers can be affected by other processes that can deposit or erode ice. One process we need to understand is the migration history for the large spiraling troughs that occur across the ice cap, which tend to have asymmetric wall slopes and reliefs. The leading theory suggests that their migration is driven by ice ablation from winds that flow down the higher trough wall, and deposition (and cloud formation) when the wind hits the trough floor and decelerates. We present an updated record of cloud coverage across the ice cap using orbital images spanning ~18 Earth-years and analyze ~3000 trough cross-sections to compare trough shape to cloud location. We find regions with clouds often correlate with trough shapes associated with modern-day sublimation-deposition cycles (wall asymmetry), but often asymmetric troughs have no clouds, or the troughs are symmetric. The fact that trough shape changes across the ice cap suggests ice transport processes are variable and need to be considered when interpreting paleoclimate.

1 Introduction

[1] The polar regions of Mars are composed of atmospherically deposited water ice and dust layers (Cutts, 1973) that record Mars' climate and hydrosphere over the lifetime of the deposits. These deposits can be divided into the South Polar Layered Deposits (SPLD) and the North Polar Layered Deposits (NPLD), of which the NPLD are younger and better characterized (Herkenhoff and Plaut, 2000; Laskar et al., 2002, 2004; Levrard et al., 2007). Like terrestrial polar ice caps, the thickness and composition of individual layers potentially offer insight to insolation-controlled climatic variations in the deposition of ice and dust on Mars (Smith et al., 2018). Understanding the stratigraphic record of these deposits is therefore important for understanding

modern Martian climate, the relationship between climate and surface processes, and volatile reservoirs on Mars (e.g., Diniega and Smith, 2020; Smith et al., 2020).

[2] At the north pole, the NPLD is a part of Planum Boreum, the northern polar plain on Mars consisting of a low-albedo sand and ice deposit (Malin & Edgett, 2002), and is a near-circular structure stretching ~1,000 km across and ~3 km above the surrounding landscape (Tanaka et al., 2008). The upper layers of the NPLD are exposed by spiral troughs, ~400 m to ~1000 m deep depressions that spiral counterclockwise (Howard et al., 1982). In cross-section, these troughs have been shown to have a high elevation and low elevation side, where the high-side is generally equator-facing, has a low albedo and is characterized by layered terrain, whereas the low-side is generally pole-facing, has an intermediate albedo (between that of the high-side and the inter-trough regions) and has a mantling that is referred to as banded terrain (Howard et al., 1982). Early studies of exposed layering in trough walls attempted to use ice layer thickness as a record of ice and dust deposition rates driven solely by changes in Mars' orbit and axial tilt, not accounting for lateral ice transfer (Cutts & Lewis, 1982; Fishbaugh et al., 2010; Howard et al., 1982; Hvidberg et al., 2012; Laskar et al., 2002; Levrard et al., 2007). However, geomorphic and modeling studies of individual troughs have shown that they migrate poleward through a combination of lateral ice transport by wind and insolation-driven sublimation (i.e., Bramson et al., 2019; Howard et al., 1982; Smith and Holt, 2010). Smith and Holt (2010) used radar data from the Shallow Radar (SHARAD) instrument onboard the Mars Reconnaissance Orbiter (MRO) to show that subsurface geometry and layering within the NPLD was also indicative of constructional trough migration, likely due to wind transport and atmospheric deposition. As such, this large-scale lateral ice transport on the NPLD will affect apparent deposition rates and layer thicknesses through time (Howard et al., 1982; Howard, 2000).

[3] Based on observations as well as modeling studies, the general conceptual model for trough migration is that ice is laterally transported through cyclic step migration driven by katabatic winds, which cause katabatic (or hydraulic) jumps in regions where wind rapidly decelerates (Smith et al., 2013), combined with ice loss from sublimation (predominantly on the equator-facing trough slopes) (Bramson et al., 2019). Katabatic winds are some of the most common winds on long, planetary slopes and are most often found on Earth near elevated ice sheets. Lied (1964) and Pettré and André (1991) identified clouds associated with katabatic jumps in Antarctica, and similar clouds were identified within the spiral troughs, leading to the hypothesis that clouds were evidence of active sublimation and deposition (Smith et al., 2013). Smith et al. (2013) examined over 10-years of Thermal Emission Imaging System (THEMIS) imagery to map near-surface clouds across the NPLD to identify trends in their timing, location, and morphology. They showed that clouds occurred between L_s 24 and L_s 102, with the highest frequency of coverage occurring around the Martian summer solstice (L_s 80-90) (Smith et al., 2013). Near-surface clouds were also found to form predominantly near the spiral troughs and were either transverse or parallel to the trough, indicating cloud formation was strongly influenced by topography (Smith et al., 2013). Their estimates of Froude numbers, wind velocity, and wind depths based on locations with cloud presence were found to be consistent with conditions associated with katabatic wind on Earth (Smith et al., 2013).

[4] Taken together prior work suggests that clouds serve as a proxy for modern-day lateral ice transport and spiral trough migration due to katabatic winds (Smith et al., 2013). However, the conclusions made by Smith et al. (2013) were based on data taken over ~10 years of the Martian cloud record, whereas there are now 18 years of data. Also, the katabatic wind-driven sublimation and deposition model assumes troughs have asymmetric wall reliefs, with a high-side

(sublimation) and a low-side (deposition), but the variability in trough morphology across the entire NPLD is unknown. Here, we expand on the work of Smith et al. (2013) by building an updated cloud atlas to understand where and how frequently clouds occur on the NPLD. We then test whether there are regional patterns in surface trough morphology, as regions have previously been distinguished across the NPLD based on their surface characteristics and subsurface layering (Smith & Holt, 2015). Lastly, we investigate if troughs with persistent cloud coverage over the last ~20 years are morphologically different (i.e., comparing cross-section shape, wall slopes, relief) than troughs in regions of inactive or no clouds.

2 Methods

2.1 Trough Cloud Imagery

[5] As of June 2022, there were 13,857 Thermal Emission Imaging System (THEMIS) visible light spectrometer (VIS) images of the Martian north polar region (northward of 82°) available on Arizona State University's Mars Image Explorer for Mars years 26–35 (Christensen et al., 2004). We examined each of these THEMIS VIS images for quality, the presence or absence of clouds, and cloud type (when present).

[6] To quantify image quality, we assigned a metric gauging whether the image was visually clear enough to distinguish clouds. This metric was based primarily on if surface features could be visibly distinguished in the image (e.g., pitting, craters, trough wall layers, trough edges, striations, etc.). A ranking of 0 means the surface features are clear and high-resolution; 1 means surface features are visible but less resolved in some way (e.g., slightly blurred, washed out, blocked by some visual artifacts, etc.); 2 means the surface features are not at all distinct or blocked out by large visual artifacts, and the image is classified as too noisy to credibly decide if clouds

are or are not present. We only used images with a rank of 0 and 1 for subsequent analyses, though all images and their assigned rankings can be found in the associated data repository.

[7] Images were then classified as either having cloud presence or absence, on a yes/no scale. To state “yes”, the cloud’s edge must be distinct from the NPLD surface, so as not to confuse the cloud with other surface features. This was particularly important for images with a noise rank of 1. If there was doubt if the feature is a cloud (e.g., due to a soft or no cloud boundary with the surface and/or image defects on top of the potential cloud), that image is classified as “no” in this analysis. If clouds were identified they were classified into three broad categories: trough-parallel clouds (similar to the low-altitude clouds with an elongated structure located parallel to the NPLD troughs identified in Smith et al. (2013)), wispy clouds, and general cloudiness. When visible,

other related cloud features were noted, such as the presence of undulations, or linear cloud structures. Examples of some of these cloud types and features can be seen in Figure 1.

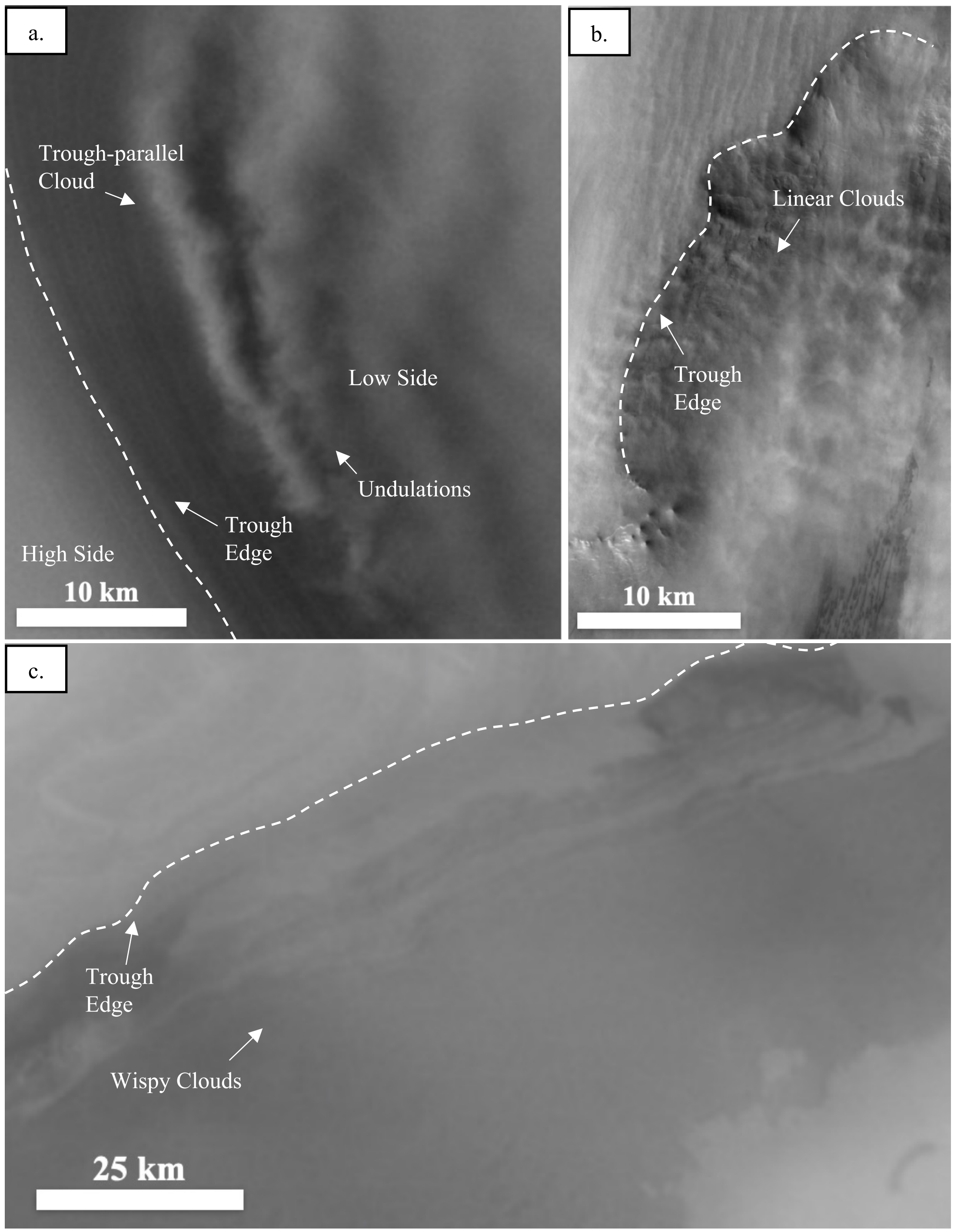

Figure 1. a.) THEMIS image V12325004 with trough-parallel, undular trough clouds, located in R3. Note the trough-parallel cloud is located on the low side of the trough. b.) THEMIS image V37081012 with linear trough clouds, located in R2, categorized as general cloudiness for this study. c.) THEMIS image V64157020 with wispy trough clouds in R2, categorized as general cloudiness for this study.

2.2 NPLD Trough Geometry

[8] We identified differences between trough morphology across the NPLD using cross-sectional analysis. We extracted 3,192, 35 km long cross-sectional trough profiles, with profiles taken every 5 km down-trough perpendicular to the trough thalweg. We used a HRSC and MOLA Blended 200m DEM (v2) (Fergason et al., 2018) resampled to 1000m/pixel, to reduce noise but retain trough shape information. Our specific resampling ratio was chosen by comparing unsampled (200m/pixel) trough metrics to resampled profiles at 500m/pixel, 1000m/pixel, 2000m/pixel, and 3000m/pixel (larger resampling sizes would compromise our 5 km profile spacing). The metric values for each resampling ratio were compared to the original unsampled ratio (200m/pixel) metric values, selecting for the largest resampling ratio that did not have statistically different results from the unsampled ratio, using a Mann-Whitney *U* Test (Mann & Whitney, 1947). This unsampled and resampled comparison was done for two different troughs (~50 different profiles) on the NPLD in region 1, a simple trough that had roughly the same cross-sectional shape for 115 km and a complex trough that changed shape frequently, in order to select a ratio that would properly capture both simple and complex trough metrics.

[9] We then calculated various trough metrics for every trough profile. To do this, all extracted trough profiles were mapped with a polynomial fit to smooth the trough profile. This

allowed us to automatically identify the trough shoulder points (A and B in Figure 2) by calculating the second derivative of the polynomial, and the trough minimum point (C in Figure 2) by calculating the first derivative of the polynomial. Our trough metrics, illustrated in Figure 2, were pole-facing relief (A minus A'), equator-facing relief (B minus B'), relief difference (the difference between A minus A' and B minus B'), pole-facing slope (average slope between A and C), equator-facing slope (average slope between B and C), width (B' minus A'), and depth (the average of A minus A' and B minus B').

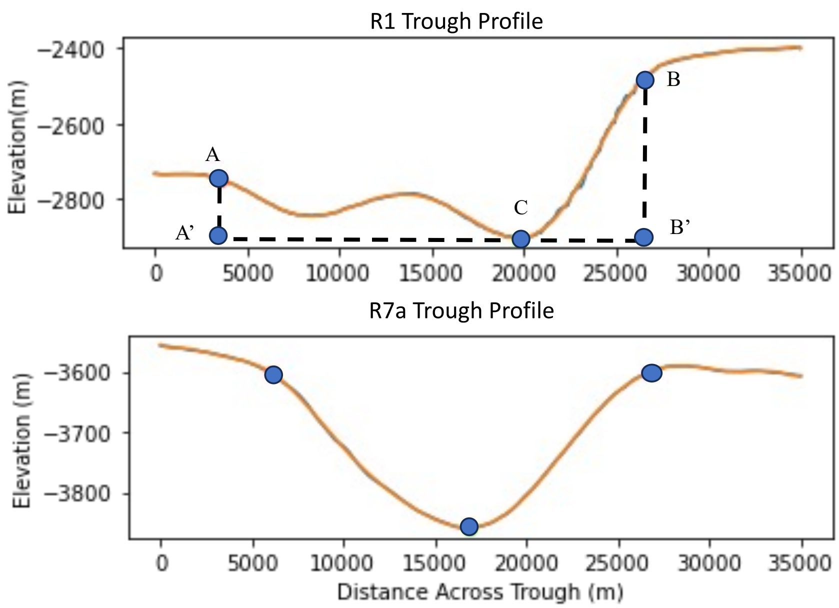

Figure 2. Examples of trough profiles (location of profiles shown in Figure 3) with key trough locations marked (blue circles) that were used to calculate the Pole/Equator relief, relief difference, Pole/Equator slope, width, and depth. Pole-facing slope is calculated from point A to C; equator-facing slope from point B to C; pole-facing relief is calculated as the distance from point A to A'; equator-facing relief is the distance from B to B'; relief difference is the difference between pole-facing and equator-facing relief; depth is the averaged relief value; width is the distance from A' to B'. Note the distinct shape differences between the two troughs, specifically that

the R1 trough has notably asymmetric relief height while the R7a trough has symmetric relief height. The R1 trough also has a central peak (often referred to as a central promontory, (Smith & Holt, 2015)) between points A and C. Vertical exaggeration ~ 1/20 for the R1 trough profile and ~1/30 for the R7a profile.

3 Results

3.1 Updated NPLD Cloud Atlas

[10] Our study identified ~800 THEMIS images out of the total ~13,800 that had clouds (Figure 3, inset), and of those, ~400 were identified as near-surface trough-parallel clouds (black circle, Figure 3), with ~33% of those being undular trough-parallel clouds (Figure 1a). Of the remaining images, ~5% contained linear cloud features (Figure 1b), ~16% contained wispy cloud features (Figure 1c), and the remainder showed general cloudiness. As seen in Figure 3, cloud coverage across the NPLD is not uniform, both for clouds in general (white points) and for trough-parallel clouds (black points). Most clouds were observed to be associated with troughs and either centered around the pole or seen on the outer margins of the deposit. In terms of total cloud observations from all THEMIS imagery (Table 1), region 1 has the highest percentage, with ~9%, followed by regions 2, 3 and 4 (~6-7%), and then region 5 (~4%). Region 7a and 7b only had ~1% and there were no clouds observed in region 6. When normalized by the total number of images with clouds (726 images), almost 30% were in region 3, 23% were in region 1, and regions 2, 4, and 5 had 12 to 17%. The remaining regions had less than 5% (Table 1). When considering trough-parallel clouds only, regions 1 and 3 had the highest percentage when normalized by all THEMIS images (~4.5%), which includes ~60% of all identified trough-parallel clouds (Table 1). Regions 2 and 4 had ~3%, followed by region 5 (2%). Regions 6 and 7a and 7b, all broadly within the

Gemina Lingula region of the NPLD, had very few to no trough parallel cloud observations (0%, 0.2%, and 0% respectively). Taken together, regions 1 and 3 tend to have the highest number of clouds, including trough-parallel clouds, followed by regions 2, 4 and 5. Regions 6 and 7 (a and b) have few to no clouds. This low frequency of clouds is important to note as region 7a does have a significant number of troughs per area.

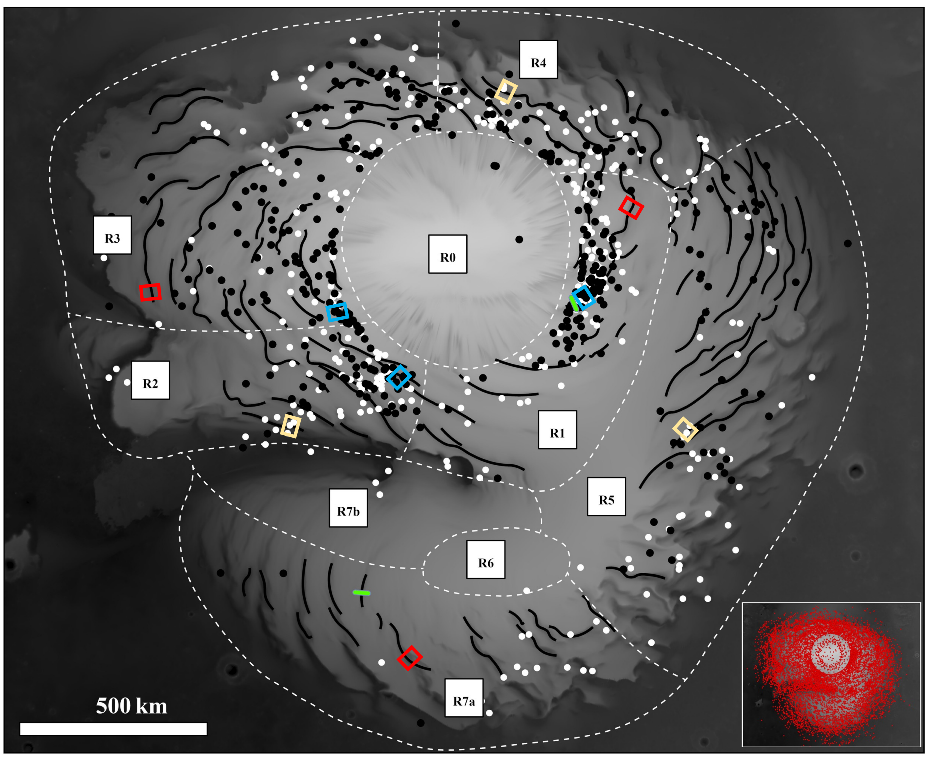

Figure 3. A map of the NPLD where THEMIS images with trough-parallel clouds (black circles) and general cloudiness (white circles) were identified in this study. The green lines indicate the location of the R1 and R7a trough profiles displayed in Figure 2. The red outlines correspond to the profile metric data classified as “No Clouds” for our statistical testing shown in Table 3. The yellow outlines correspond to the profile metric data classified as “General Cloudiness” for our statistical testing shown in Table 3. The blue outlines correspond to the profile metric data

classified as “High Frequency of Trough-Parallel Clouds” for our statistical testing shown in Table 3. The sub-figure displays the locations of all THEMIS imagery investigated in this study, marked by red circles.

Regions	**Number of Images**	**Number of Images w/ TP Clouds**	**Ratio TP Clouds/Total Images in Region**	**Number of Images w/ Clouds**	**Ratio Clouds/Total Images in Region**	**Trough Cloud Types Identified in Region**
Region 1	1,874	84 (22%)	0.045	164 (23%)	0.088	General, wispy, linear, **TP (high presence), undular TP**
Region 2	1,994	55 (14%)	0.028	126 (17%)	0.063	General, wispy, linear, **TP, undular TP**
Region 3	3,021	141 (37%)	0.047	206 (28%)	0.068	General, wispy, linear, **TP (highest presence), undular TP**
Region 4	1,648	49 (13%)	0.03	113 (16%)	0.069	General, wispy, **TP, undular TP**
Region 5	2,499	47 (12%)	0.019	88 (12%)	0.035	General, wispy, linear, **TP, undular TP**
Region 6	120	0 (0%)	0	0 (0%)	0	No clouds seen
Region 7a	1,605	4 (1%)	0.002	23 (3.1%)	0.014	General, wispy, **TP (lowest presence)**
Region 7b	890	0 (0%)	0	6 (0.8%)	0.007	General, wispy
TOTAL	**13,857**	**380**	**0.027 (2.7%)**	**726**	**0.052 (5.2%)**	

Table 1. Number of THEMIS images investigated in this study broken down by region (based on regions delineated in Smith and Holt, 2015) as well as the number and percentage of those images where any clouds, and specifically trough-parallel clouds, were observed. Trough-parallel is shortened to TP in this table.

[11] Cloud coverage has seasonal variations and trends over time (Figure 4b). Similar to seasonal patterns identified by Smith et al. (2013) for Mars years 26 – 31, the earliest clouds each year were observed during Mars' north polar spring, with the highest frequency of clouds occurring slightly later in the spring. No clouds are identified during Mars' north polar winter, or dust storm season. It is important to note that almost no images are taken during Mars' north polar fall or winter, including during dust storm season, and the few that exist are entirely dust covered, so there is no way visually to note whether trough clouds are in fact present during this time. Additionally, there are fewer THEMIS images earlier in the Mars year as compared to the high frequency of imaging in late spring to early summer (Figure 4b). This means that locations on the NPLD that could be more prone to cloud coverage earlier in the Mars year are being imaged less frequently compared to those prone to cloud overage later in the season. Both factors limiting imaging in specific Mars seasons should be noted as potential causes of sampling bias in our

results, where we are potentially missing clouds present early or later in the Mars year due to a lack of THEMIS imaging coverage.

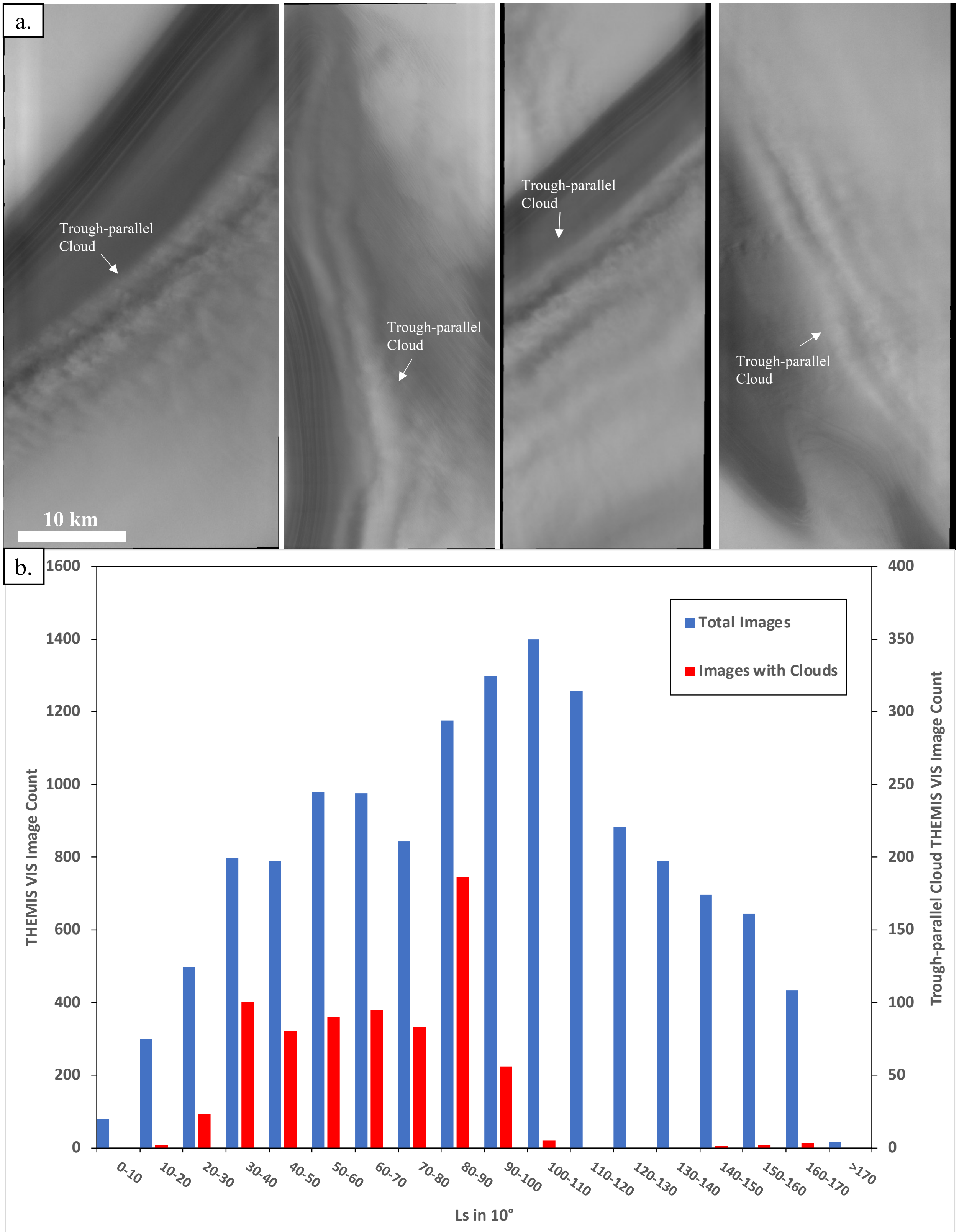
a.
Trough-parallel Cloud
Trough-parallel Cloud
Trough-parallel Cloud
Trough-parallel Cloud
10 km
b.
Total Images
Images with Clouds
THEMIS VIS Image Count
Trough-parallel Cloud THEMIS VIS Image Count
Ls in 10°
0-10
10-20
20-30
30-40
40-50
50-60
60-70
70-80
80-90
90-100
100-110
110-120
120-130
130-140
140-150
150-160
160-170
>170

233

Figure 4. a.) Additional examples of THEMIS images with trough-parallel clouds; from left to right V29043038, V45756001, V62430037, V78928031. b.) Temporal histogram of clouds. The ~13,500 THEMIS VIS images were examined for clouds over Mars years 26–35 (blue bars). ~400 images capture clouds like those depicted in a) and in Figure 1a (red bars). Clouds imaged by THEMIS begin after Ls 14, spike between Ls 30 and 40, peak between Ls 80 and 90, then taper off sharply near Ls 100. The last trough-parallel cloud is observed at Ls 168.

3.2. Regional Trough Profile Morphology

[12] We compared our trough profile metrics, as defined in Section 2.2, across the NPLD to identify any regional trends (Figures 5-8; S1). We found that trough profile depths (Figure 5a) varied between ~30 m and ~980 m across the entirety of the deposit. This is similar to depths noted by Pathare and Page (2005), who report depths of 200-900 m for the select troughs they investigated. Regions 1 and 5 had similar depth distributions with most troughs being between 100 m and 300 m deep, with a mean of ~210 m (median ~208 m). Regions 3 and 7a had a larger range of depths, ~100 m to 500 m, with a mean depth of ~260 m for region 3 (median ~250 m) and ~308 m for region 7a (median ~282 m). Region 4 had generally deeper troughs, ranging between ~200 m and ~600 m, with a mean of ~365 m (median ~354 m). Region 2 had the most uniform distribution of trough depths, ranging between ~100 m and ~600 m (mean ~326 m and median ~ 313 m).

[13] Trough profile widths (Figure 5b) ranged from ~7 km to ~34 km across the deposit. Most of the troughs in regions 2 and 5 were between ~10 km and ~27 km, with a mean width of ~18 km (median ~17 km). Regions 3 and 4 had generally larger trough widths than the troughs in region 2 and 5, with values between ~13 km and ~30 km (mean of ~20 km and median of ~21 km

for both regions). Region 1 had the narrowest troughs on average, with most between ~5 and ~25 km (mean and median ~15 km), and the narrowest troughs observed across the NPLD were those in Region 1. Region 7a was the most uniformly distributed, with widths between ~10 km and ~33 km (mean ~19 km, median ~18 km).

[14] Pole-facing wall slopes (Figure 6a) ranged from ~0.006 to ~5 degrees across the NPLD, but in all regions most of the walls were between 0.25 and 3.5 degrees with a mean (and median) of ~1-1.7. Equator-facing wall slopes (Figure 6b) had a similar range of values as compared to pole-facing wall slopes (~0.006 to ~7 degrees), though there was more variability by region. Regions 3 and 5 had shallower equator-facing wall slopes on average (mean ~1.6 to 1.8 degrees and median ~1.6 to 1.7 degrees), while region 1, 4, and 7a tended to be slightly steeper, with means of ~2, ~2.6, and ~2.1 degrees, respectively. Region 2 was more broadly distributed, with wall slopes falling between ~0.4 and ~6 degrees and had a mean of ~2.6.

[15] Pole-facing relief (Figure 7a) ranged from ~0.5 m to ~744 m across the NPLD, with regions 1, 3, and 5 having reliefs between ~0 m and ~350 m, though regions 3 and 5 have means of ~150 m while region 1 has a mean ~126 m. Regions 2, 4, and 7a had a broader distribution of reliefs (between ~0 m and ~500 m) and were steeper and their average reliefs ranged from ~215-240 m (Figure 7a). Equator-facing wall relief (Figure 7b) ranged from ~0.4 m to ~1280 m across the deposit, but the distributions in relief varied more by region than those for pole-facing relief. Equator-facing reliefs in region 1 fell between ~50 and ~600 m (with a mean of ~300 m), but had a bimodal distribution with a larger peak at ~200 m and a second smaller peak at ~400 m. Equator-facing reliefs for regions 3 and 7a ranged between ~50 m and ~750 m, with a mean of ~361 m and ~374 m respectively (median ~345 m and ~352 m). Region 5 had a slightly narrower distribution of equator-facing reliefs as compared to other regions, ranging from ~50 m to ~450 m, though the

mean and median (~274 m and ~270 m) were close in value to those of region 1. Regions 2 and 4 tended to have higher equator-facing reliefs (means of ~436 m and ~505 m respectively), though Region 2 was slightly bimodal with a main peak at ~400 m and a smaller peak at ~700 m.

[16] When investigating wall asymmetry (i.e., differences in wall relief across a trough profile) (Figure 8a), we found that asymmetry ranged from ~0 m to ~800 m across the NPLD. As expected from its distributions in pole- and equator-facing relief, relief differences in region 1 were bimodally distributed, with peaks at ~100 m and ~300 m. The different peaks appear spatially distributed, with troughs in R1 located closer to R4 all having larger relief differences and those closer to R2 having smaller relief difference. The values of those troughs located near R4 also matches R4 relief difference values closely. Regions 2 and 3 were more widely and uniformly distributed, with relief differences varying between ~100 m and ~800 m. Region 4 had the largest relief differences, averaging ~300 m, while region 5 had the smallest (~130 m). Region 7a was the most right-skewed, having the highest density of trough profiles with negligible asymmetry. Based on the distribution of trough metrics investigated herein, there is not a clear pattern that emerges regarding regional distinctions in trough morphology. For example, the scale of troughs in regions 1 and 5 based on their width and depth are quite similar, but most troughs in region 5 have relief differences of ~100 m whereas region 1 is more bimodal, with trough differences of ~100 m or ~300 m. Similarly, troughs in regions 2 and 7a are also comparable in size regarding their width and depth, but region 2 has generally greater relief differences and a greater distribution of wall

slopes.

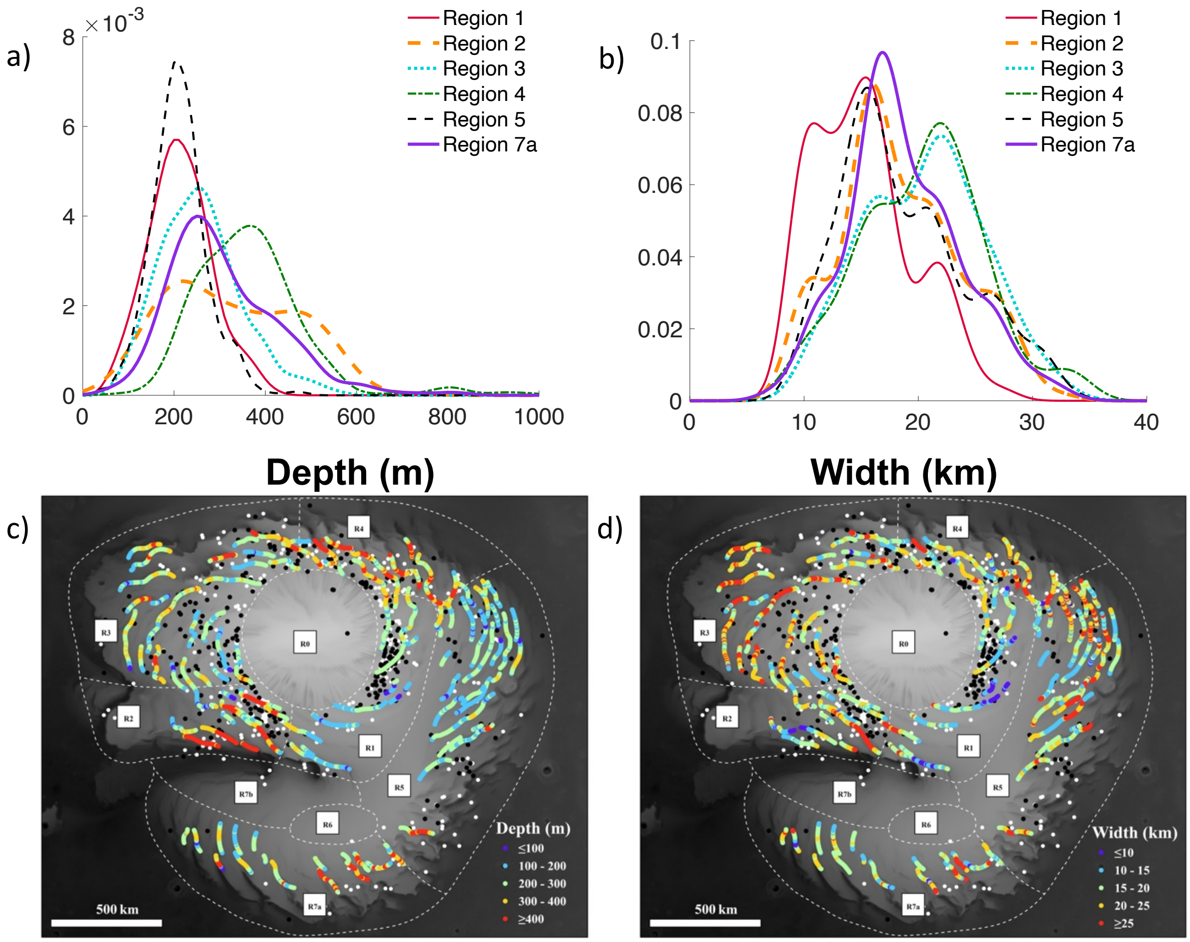

Figure 5. a) Probability distribution function (PDF) curves of the depth data, plotted by region. R0, R6, and R7b are not included as they have no troughs. b) Same as (a) but for trough width. c) A map of the NPLD with trough depth data plotted as compared to THEMIS images with trough-parallel clouds (black circles) and general cloudiness (white circles) that were identified in this study. d) same as (c) but for width.

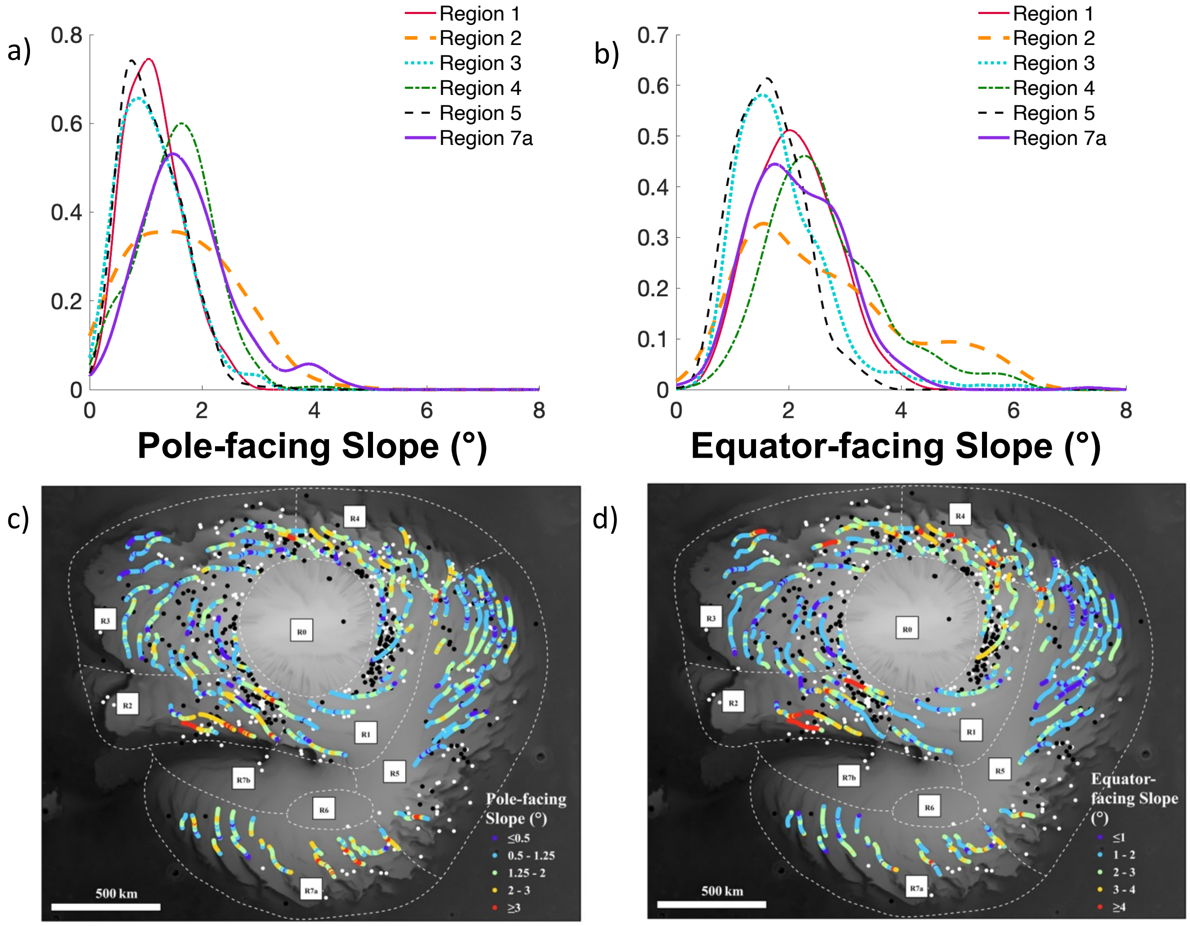

Figure 6. a) Probability distribution function (PDF) of the pole-facing slope data, plotted by region. b) same as (a) but for equator-facing slope. c) A map of the NPLD with trough pole-facing slope data plotted as compared to THEMIS images with trough-parallel clouds (black circles) and general cloudiness (white circles) that were identified in this study. d) same as (c) but for equator-facing slope.

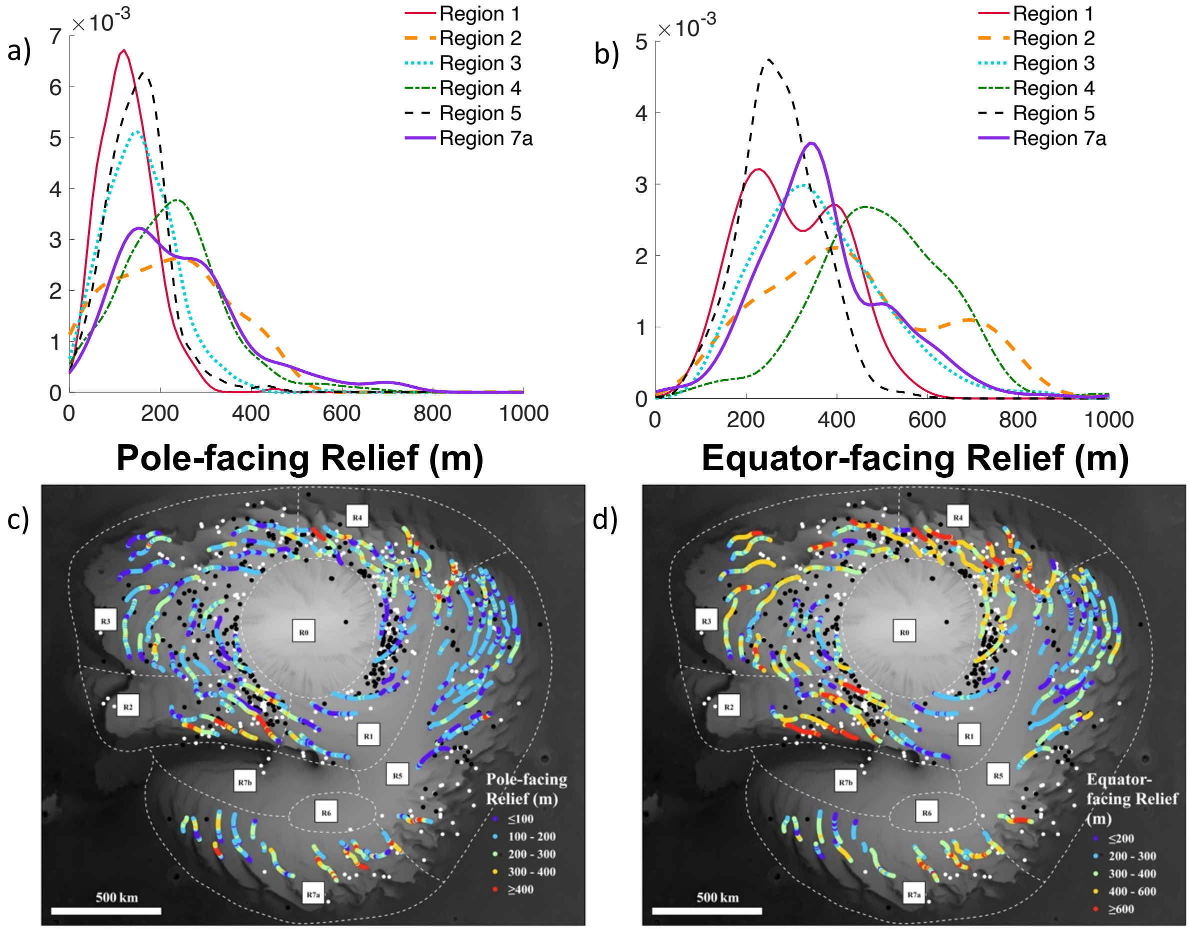

Figure 7. a) Probability distribution function (PDF) curves of the pole-facing wall relief data, plotted by region. b) same as (a) but for equator-facing wall relief. c) A map of the NPLD with trough pole-facing wall relief data plotted as compared to THEMIS images with trough-parallel

clouds (black circles) and general cloudiness (white circles) that were identified in this study. d) same as (c) but for equator-facing wall relief.

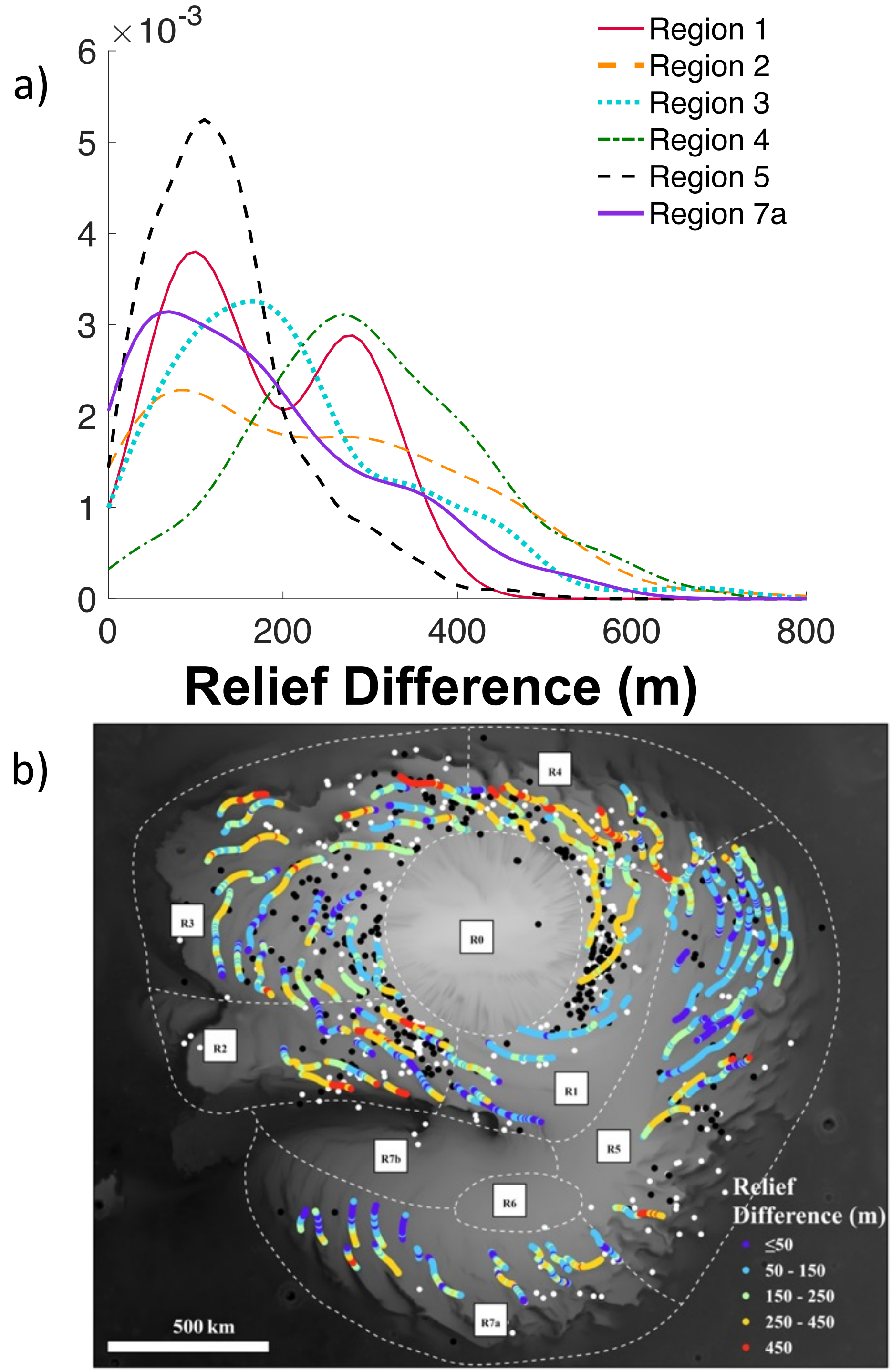

Figure 8. a) Probability distribution function (PDF) curves of the pole-facing relief data, plotted by region. b) A map of the NPLD with trough wall relief difference data plotted as compared to THEMIS images with trough-parallel clouds (black circles) and general cloudiness (white circles) that were identified in this study.

[17] We also conducted statistical testing to identify if our trough metrics were significantly different from each other when grouped by region. First, we used a Kruskal-Wallis Test (Kruskal & Wallis, 1952), a non-parametric test to identify if two or more datasets originate from the same distribution, to identify if, for example, trough profile widths from one region were significantly different from another region. If the p-value calculated from this test was below 0.05 for 95% confidence, we could reject the null hypothesis that the distribution of a given metric was not significantly different between regions. As this test only identified if *any* of the regions had significantly different distributions and did not identify which regions were significantly different from one another, a post-hoc Dunn's test was conducted to identify which specific regions were significantly different (Table 2). We confirmed that while some regions are statistically different from one another (e.g., regions 1 and 2 are significantly different across all but one metric), those same regions are similar to other regions based on individual metrics (e.g., region 2 can't be distinguished from region 5 by width or regions 3 for relief difference). As such, we find that the regions delineated by Smith and Holt (2015), which were based on a combination of surficial characteristics (i.e., regional topographic slope, trough wavelength, terrain type) and subsurface (i.e., reflector morphology) characteristics, were not readily distinguishable by the metrics investigated here.

Width	**R1**	**R2**	**R3**	**R4**	**R5**	**R7a**		**Depth**	**R1**	**R2**	**R3**	**R4**	**R5**	**R7a**
R1		**S**	**S**	**S**	**S**	**S**		**R1**		**S**	**S**	**S**	NS	**S**
R2			**S**	**S**	NS	NS		**R2**			**S**	**S**	**S**	NS

R3				NS	**S**	**S**		**R3**				**S**	**S**	**S**
R4					**S**	**S**		**R4**					**S**	**S**
R5						NS		**R5**						**S**
Pole Slope	**R1**	**R2**	**R3**	**R4**	**R5**	**R7a**		**EQ Slope**	**R1**	**R2**	**R3**	**R4**	**R5**	**R7a**
R1		**S**	NS	**S**	NS	**S**		**R1**		NS	**S**	**S**	**S**	NS
R2			**S**	NS	**S**	NS		**R2**			**S**	**S**	**S**	NS
R3				**S**	NS	**S**		**R3**				**S**	**S**	**S**
R4					**S**	NS		**R4**					**S**	**S**
R5						**S**		**R5**						**S**
Pole Relief	**R1**	**R2**	**R3**	**R4**	**R5**	**R7a**		**EQ Relief**	**R1**	**R2**	**R3**	**R4**	**R5**	**R7a**
R1		**S**	**S**	**S**	**S**	**S**		**R1**		**S**	**S**	**S**	**S**	**S**
R2			**S**	NS	**S**	NS		**R2**			**S**	**S**	**S**	**S**
R3				**S**	NS	**S**		**R3**				**S**	**S**	NS
R4					**S**	NS		**R4**					**S**	**S**
R5						**S**		**R5**						**S**
Relief Diff	**R1**	**R2**	**R3**	**R4**	**R5**	**R7a**							
R1		**S**	NS	**S**	**S**	NS							
R2			NS	**S**	**S**	**S**							
R3				**S**	**S**	**S**							
R4					**S**	**S**							
R5						**S**							

Table 2. Results of statistical testing of trough metrics as compared between regions. If the distributions of the datasets are significantly different from one another the value S, short for *Significant,*

is recorded; if the distributions of the datasets are not significantly different from one another the value NS, short for *Not Significant,* is recorded.

3.3. Linking Cloud Presence with Trough Morphology Metrics

[18] To understand how trough-parallel cloud presence or absence linked to our trough morphology metrics, sections of the NPLD were visually identified that had high trough-parallel cloud presence (blue boxes, Figure 3), low trough-parallel cloud presence but high presence of other cloud types (yellow boxes, Figure 3), and both low trough-parallel cloud and other cloud type presence (red boxes, Figure 3). Three 25 km long sections of these three subtypes, consisting of 5 trough profiles each, were selected to compare metrics in these regions and note if they were statistically significantly different from one another. We followed the same statistical procedure as outlined in section 3.2 (i.e., a Kruskal-Wallis Test followed by a post-hoc Dunn's Test if the null hypothesis could be rejected). We found statistically significant links (i.e., p-values < 0.05 with 95% confidence) between cloud presence and trough wall relief difference (Table 3), as there was a significant difference between all three subtypes, but in general, cloud subtype did not have statistically significant trends with trough profile morphology (Table 3). For example, for relief difference in Figure 8b, we see that when trough-parallel clouds are present (black dots), wall asymmetry is typically >50m. This is especially true in region 1, where trough-parallel clouds are associated with wall relief differences between ~250 and ~450 m, such that wall morphology appears like that in Figure 2a. However, in many troughs across the NPLD, there are similarly asymmetric walls (e.g., region 7a) and no trough-parallel clouds were observed. There is also a region in region 2 (85.8 N, 330 E), where wall asymmetry is negligible (< 50 m and with cross-sectional

profiles like that in 3b), but a cluster of trough-parallel clouds were co-located. This region did however have a notably deep (>400 m, Figure 5c) and wide (>25 km, Figure 5d) section of trough.

Trough Metric	No Clouds vs General Cloudiness	No Clouds vs Trough-parallel Clouds	General Cloudiness vs Trough-parallel Clouds
Depth	**Significant**	**Significant**	Not Significant
Width	**Significant**	**Significant**	Not Significant
Pole-Facing Slope	Not Significant	Not Significant	Not Significant
EQ-Facing Slope	**Significant**	Not Significant	Not Significant
Pole-Facing Relief	Not Significant	Not Significant	Not Significant
EQ-Facing Relief	**Significant**	**Significant**	Not Significant
Relief Difference	**Significant**	**Significant**	**Significant**

Table 3. Table of the results of our statistical testing between the three subsections identified with different cloud presence/absence, outlined in Figure 3. If the distributions of the datasets are significantly different from one another the value *Significant* is recorded; if the distributions of the datasets are not significantly different from one another the value *Not Significant* is recorded.

4 Discussion

4.1 Cloud Distribution Across the NPLD

[19] Smith et al. (2013) looked at ~8,500 optical images from Mars years 26-31 (mostly from THEMIS but also from the High Resolution Stereo Camera (HRSC), Mars Orbiter Camera (MOC), Context Imager (CTX) and the High Resolution Imaging Science Experiment (HiRISE)) and identified ~370 cloud images with elongated structures and of those ~350 were classified as having trough-parallel clouds in THEMIS images and another 6 were identified in other imagery (~4%). Our study looked at 13,857 THEMIS images, which extended the cloud survey of Smith et al. (2013) by eight more Earth years (Mars years 26 – 35), and we found ~400 images with definitive trough-parallel clouds (~2.7%). The fact we find ~25% less images with trough-parallel cloud occurrence than previously is likely due to our image quality assessment, such that any

images where clouds might have been present, but image quality precluded a definitive 'yes', were not included in our final counts (but those images are included in the complete atlas; see Availability Statement for link). However, like Smith et al. (2013), we find that even over our longer observation period, cloud occurrence is rare across the NPLD. In terms of seasonality, we see the presence of clouds starting around L_s 10 – 20 and ending by L_s 168. This is a later end date than seen in Smith et al (2013) where the last trough cloud was observed at L_s 102, but it is important to note that we only observe six clouds after L_s 102, only two of which are trough-parallel. Most cloud observations occurred between L_s 30 – 100, with the highest frequency between L_s 80 – 90 (Figure 4b). This is similar to Smith et al. (2013) (see their Figure 9), suggesting cloud patterns and occurrence have overall been consistent over the last ~20 Earth years.

[20] Our map shows that cloud coverage across the NPLD for Mars years 26 – 35, specifically trough-parallel clouds, is not uniform (Figure 3). Regions with the highest trough-parallel cloud frequency (i.e., regions 1, 2, 3, and 4) are mainly those that contain troughs clustered together centrally on the main lobe of the NPLD, while the outer regions of the deposit, especially the outer lobe of Gemina Lingula (regions 5 and 7a) have about half as many trough-parallel clouds. These regions do however contain troughs. Regions 6 and 7b have few to no trough-parallel clouds, but also contain few troughs. Meso-scale atmospheric simulations by Smith and Spiga (2018) showed that cloud counts by region roughly correlated with increases in wind speed, though cloud observations in regions 1-3 tended to lag peaks in wind speed. Interestingly, all the regions they looked at (1-5 and 7a) had max wind speeds of ~10 m/s (though region 2 was closer to 13 m/s). It is important to note that the resolution of the meso-scale model did not resolve the relatively steeper high-side slopes of the troughs, which limited velocity values. Higher resolution modeling done by Smith and Spiga (2018) of an individual R1 trough found that winds could reach close to 20

m/s. They suggested that cloud formation requires both strong katabatic winds, but also super saturated water vapor, and that water vapor is limited until the seasonal CO_2 retreats poleward (after L_s ~80 for the central regions). While this helps explain the temporal variability, it does not explain why the distal regions of the deposit have so few clouds relative to the inner regions (assuming this lack of cloud presence is not due to sampling bias in THEMIS imagery coverage). But if clouds are indicators of both where winds are fast enough to lead to katabatic jumps and contain water vapor (i.e., can laterally transport water/ice mass), then we would expect that modern-day lateral transport is not occurring uniformly on the NPLD (and is mostly concentrated in regions 1, 2, 3 and 4) nor within a single trough.

4.2 Variations in Trough Geometry Across the NPLD

[21] Prior work by Smith and Holt (2015) characterized the diversity of spiral troughs across the NPLD and found that while troughs had unique evolution histories, there were regional surface and subsurface morphologic similarities that allowed them to be grouped into eight regions (Figure 3). Most of their grouping was based on subsurface observations, including trough migration paths (TMPs) (estimated by tracking subsurface reflectors and their intersection with discontinuities interpreted to be bounding surfaces created during bedform migration (Smith and Holt, 2010)), TMP depths, accumulation patterns, presence of "v-shaped" reflectors, which were later interpreted to be buried promontories (Smith & Holt, 2015), and trough initiation slopes. Surface observations mostly focused on whether layered and banded terrain was observed, trough wavelength, general trough depth, the presence of central promontories (which create a "w-shaped" trough cross-section), and extent of erosion. Smith and Holt (2015) classify region 1 as the archetypical region, with mostly asymmetric troughs (e.g., Figure 2a), region 2 was found to have deeper troughs with occasional central promontories, and region 3 was more variable in trough depth and

wavelength. The surface topography of region 4 was not discussed due to past extensive erosion and deposition. Troughs in region 5 were suggested to have initiated after widespread erosion and hence are younger than troughs in other regions. Troughs in region 7a were also affected by extensive erosion (like region 4), are less mature than those in other regions, and have a bedrock base such that migration is forced to be horizontal. Despite these differences, it is generally stated that all troughs are asymmetric in slope and elevation, having a topographic high side and low side, where the high side faces approximately equatorward (e.g., Bramson et at., 2019; Howard et al., 1982; Pathare & Paige, 2005; Smith et al., 2013; Smith & Holt, 2015).

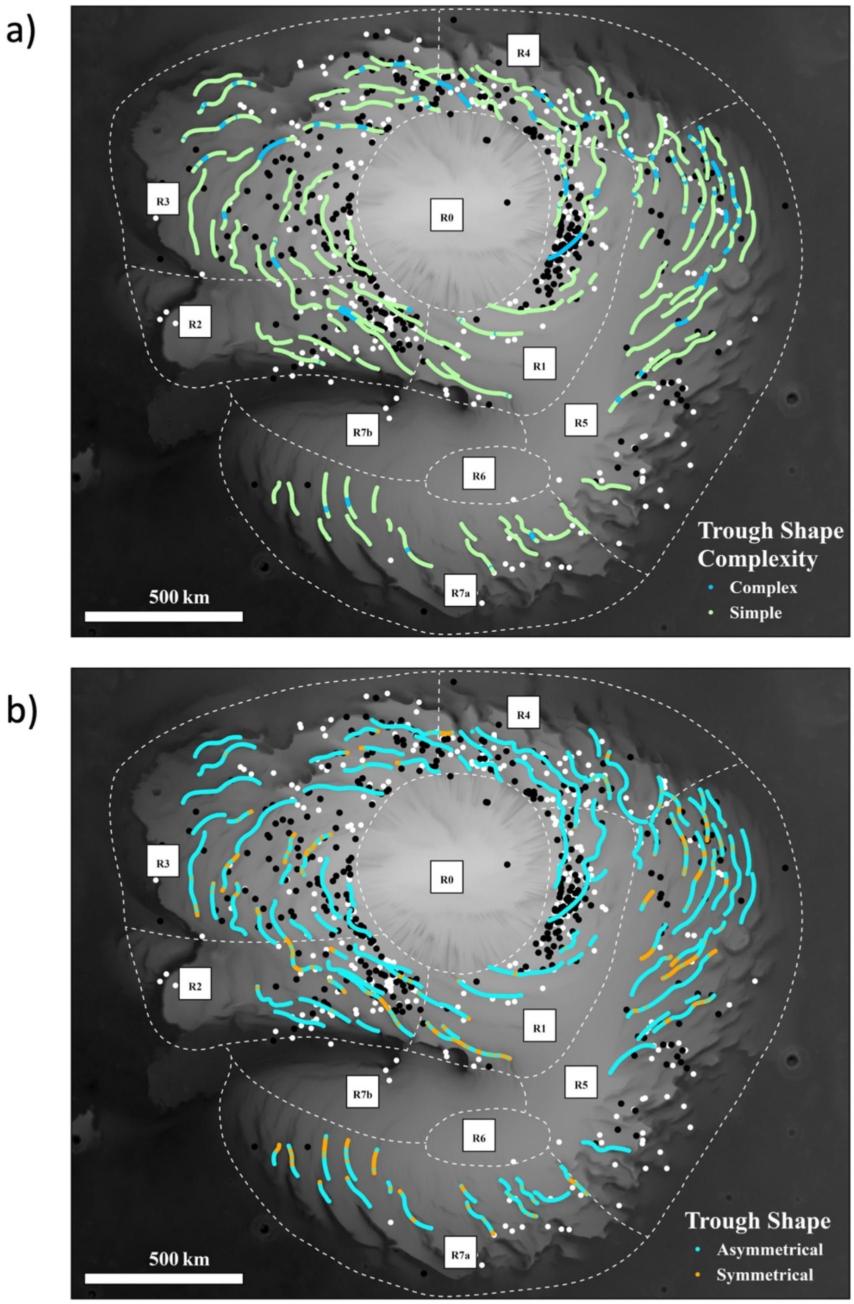

Figure 9. a) A map of the NPLD with trough shape complexity (simple versus complex) compared to THEMIS images with trough-parallel clouds (black circles) and general cloudiness (white

circles) that were identified in this study. Complex troughs included troughs with central promontories, undular features, or both. b) Same as (a) but mapping trough wall symmetry or asymmetry. Troughs were identified as symmetrical if their wall reliefs had a difference of 50 m or less.

[22] Our work looked at over 3000 cross-sections of troughs across the NPLD to further characterize regional diversity and investigate trough shape across the deposits. While most troughs have a simple u- or v-shape, there are sections of troughs that display more complex features including a "w-shape" from central promontories, undulations, or a combination of both. A section of "complex" trough profiles located in R1 correlates with a high trough-parallel cloud presence in that location (Figure 9a), specifically to undular trough-parallel clouds (Figure S2). In contrast, there are smaller sections of "complex" trough profiles in R5 that have little-to-no trough-parallel clouds nearby, and sections of "complex" trough profiles in R3 and R4 that do have trough-parallel clouds present, but less frequently than in R1. This variable linkage between the features identified in the "complex" trough profiles, including central promontories and/or undulations, and trough-parallel (often undular) clouds suggests that there may be other mechanisms driving the formation of these "complex" features.

[23] We also aimed to investigate how ubiquitous asymmetric trough cross-sections are within each region of the NPLD. This topographic asymmetry is key to the Smith et al. (2013) model for lateral ice transport and cloud formation, as ablation occurs when wind accelerates down the steeper high side of the trough and deposition occurs where the winds suddenly decelerate (i.e., where a hydraulic jump and cloud formation occurs). We find that troughs are generally asymmetric across the NPLD (87% of our cross-sections were asymmetric) (Figure 8b). However, troughs are not always entirely asymmetric (orange dots, Figure 9b), especially in regions 5 and 7a, though portions of troughs in every region were found to have some symmetric or "v-shaped" walls (R1

and R4 having much fewer compared to other regions, Figure 9b). We also find that the symmetric troughs in region 7a and 5 are similar in scale to those in other regions; this suggests these symmetric troughs are not simply undulations. It is also worth noting that regions with high trough shape complexity are located in regions with asymmetrical troughs; no regions with strong trough wall symmetry also have complex shapes. We discuss the implications for these "v-shaped" portions of troughs on ablational and depositional processes below, but it is possible these locations are surface expressions of the "v-shaped" anomalies observed in SHARAD data by Smith and Holt (2010, 2015), which were interpreted to be buried central promontories (Smith & Holt, 2015). While it is possible our "v-shaped" surface troughs and their subsurface "v-shaped" reflectors are related, it is important to note that the "v-shaped" reflectors identified by Smith and Holt (2010, 2015) were found exclusively in region 1, while we find that region 1 is one of two regions with little-to-no trough wall symmetry on the surface. More work comparing surface and subsurface features is needed to concretely say if these "v-shaped" features are linked spatially or by formation mechanism. Another possible influence on trough symmetry is the presence of small sedimentation waves, which were identified on Gemina Lingula (aka regions 7a and 7b) by Herny et al. (2014). However, we also find frequent trough symmetry in region 5 and to a lesser degree in regions 2 and 3, suggesting that sedimentation waves are not the only explanation for trough symmetry.

[24] In regard to regional morphology, we did not find that one region could be clearly distinguished from another based on the group of morphologic parameters investigated herein. However, we did find that for certain parameters, or groups of parameters, several regions were quite similar. For example, troughs in regions 1 and 5 had almost the same scale in regard to width and depth (~200 m deep and ~16 km wide) and wall slopes, and as such, were statistically indistinguishable. However, region 5 tended to have relief differences on the order of ~100 m, while

region 1 had a more bimodal distribution with relief differences around ~100 m and 300 m. As such, based on wall asymmetry they were statistically significantly different (Table 2). We also find that regions 2 and 7a generally were similar in terms of depth, width, and slope but were statistically significantly different equator-facing relief and relief difference. The size of troughs, including their width and depth, as well the height of their walls and their wall slopes, is likely a consequence of the type and/or magnitude of modern-day surface processes that causes ablation, sublimation, and deposition of ice, which is predominately driven by the atmospheric state (temperature, pressure, and wind) as well as changing CO_2 and dust cover (e.g., Bramson et al., 2019; Howard et al., 1982; Smith & Spiga, 2018). Regions that tend to be similar to one another (e.g., region 1 and 5, 2 and 7a) are geographic neighbors and thus likely experience similar insolation, wind speeds and rates of atmospheric CO_2 and water vapor deposition (e.g., Smith and Spiga, 2018; Emmett et al., 2020; Khayat et al., 2020). However, local topographic variability (e.g., ice sheet slopes, undulations in the ice, initial trough morphology, and trough spacing) likely affects smaller-scale wind patterns, which determines where and how much ice and dust accumulate (e.g., Koutnik et al., 2005; Smith and Spiga, 2018), which ultimately can affect trough shape at a given location. This local variability has also been observed in the subsurface (e.g., Smith & Holt, 2010; 2015), supporting that individual trough evolution has been variable through time and this variability needs to be considered when making interpretations about the linkage between NPLD stratigraphy and climate from a given radargram or cross-section.

[25] Additionally, the boundaries of region 1 and 4 could be re-examined based on surficial morphology. For example, the bimodal relief difference values in region 1 appear spatially distributed. Troughs closer to region 4 have larger relief differences and those closer to region 2 have smaller relief differences. We also see that the absolute values of relief difference of troughs

located near region 4, but mapped within region 1, closely match those of region 4. Other factors that could affect the regional distribution of trough geometry include differing climatic states influencing the troughs in the past as compared to the present, such as regions 5 and 7a on Gemini Scopuli, which experienced a massive erosional period linked to the formation of a later generation of NPLD troughs (Smith & Holt, 2015), or varying trough initiation properties, as initiation slope has been seen to have a strong influence on the trough wavelengths per region (Smith & Holt, 2015).

4.3 Association Between Trough Parallel Clouds and Trough Morphology: Implications for Modern-Day Surface Processes

[26] The Smith et al. (2013) cyclic step model is currently the best accepted explanation for the morphology and migration of the NPLD spiral troughs. On Earth, cyclic steps can develop under net erosional conditions (e.g., Parker & Izumi, 2000), net depositional conditions (Kostic & Parker, 2006) and equilibrium conditions (Taki & Parker, 2005). Smith et al. (2013) argue that the NPLD is a net depositional system, as a net erosional system entrains ice and water vapor as flow accelerates down the trough wall, but the load remains in suspension after the hydraulic jump (Parker & Izumi, 2000). In this case, clouds would likely not be observed, and asymmetric accumulation would not occur. The fact that Smith et al. (2013) observed trough parallel clouds in conjunction with troughs that showed morphologic evidence of ice erosion and re-deposition in their study areas led to the hypothesis that the troughs are constructional features across the entirety of the deposit. We aimed to extend their analysis to see how ubiquitous the relationship between asymmetric troughs and clouds is under modern-day climate. Based on our morphologic and statistical analysis, we find that areas with a high concentration of trough parallel clouds are also regions with trough asymmetry (especially region 1). We also find that in most cases where

symmetric or "v-shaped" portions of troughs are found, trough parallel clouds are rarely present (except for a portion of a trough in region 2). So broadly, our analysis supports the more local findings of Howard et al. (1982) and Smith et al. (2013). As our cloud record has extended cloud observations to almost 20 Earth years, and we see little change in where clouds are found, this implies that these regions have been continuously active in terms of lateral ice transport. Smith et al. (2013) estimate annual migration rates of ~20 mm/ Mars year, which would mean portions of troughs in regions 1, 2, 3, and 4 have likely moved almost 0.2 m since the start of our cloud atlas, which is at the edge of detection with HiRISE-derived topographic models.

[27] However, we did find that ~13% of the trough profiles we investigated were symmetric, which means that while a net constructional cyclic step model can explain the overall evolution and migration of the NPLD troughs, other processes are also likely at play. For example, insolation can also remove ice from trough walls (Howard, 2000), which depending on the relative amount of accumulation from the atmosphere and sublimation from insolation, could potentially result in more uniform wall heights and slopes on the pole-facing and equator-facing sides of the trough. There is also evidence for in-situ erosion in the form of pits and scarps across the deposit (Howard, 1982; Rodriguez & Tanaka, 2011; Rodriguez et al., 2021). Rodriguez et al. (2021) have theorized that with an in-situ erosion model, these pits and scarps can grow and integrate overtime to form troughs, similar to some karstic systems here on Earth. While this model cannot explain many of the other surface and subsurface observations that have been made regarding the spiral troughs (see criteria outlined in Smith et al., 2013), it is possible that in-situ erosion occurs when katabatic winds are strong enough to erode, but ice deposition does not occur (similar to the net erosional cyclic step model, discussed in reference to the SPLD in Smith et al. (2015)). Under these conditions, it is possible that previously asymmetric trough walls can become more symmetric and "v-

shaped" (i.e., winds erode down the higher wall but there no deposition on the lower wall). Many of the "v-shaped" troughs we observed are in regions 5 and 7a, which are part of Gemini Scopuli, a region that experienced a massive erosional period and has younger troughs (Smith & Holt, 2015). This might suggest troughs there were formed by a different proportion of constructional versus erosional cyclic steps or in-situ erosion compared to regions closer to the pole, or that the unique erosional climate that led to these second-generation troughs also influenced their symmetric shape. But the fact that "v-shaped" reflectors are seen in SHARAD data across the deposit (including regions 1 and 2) suggest that troughs across the deposit go through periods of time where changes in local wind speed, insolation, ability to entrain water/ice (i.e., sediment supply") can lead to more variable trough morphology. Understanding what controls this variability, the relative proportion of erosional to depositional processes that results in a given trough profile shape, and how this may have changed through time will allow us to better connect the geomorphology and stratigraphy of the spiral troughs to Martian climate processes at more local to regional scales.

5 Conclusions

[28] The creation of an extended cloud atlas, covering ~18 Earth years of THEMIS VIS imagery, combined with a detailed morphologic investigation of trough morphology across the NPLD, allowed us to better quantify more general past observations of the NPLD (e.g., Smith et al., 2013). We found that trough-parallel cloud timing and location has been consistent for ~2 decades, suggesting regions with clouds are continuously active in terms of modern-day change. This combined with estimates of annual migration rates on the NPLD, suggests that regions with clouds

would have evidence of modern-day change that could potentially be directly observed with high-resolution orbital data.

[29] We quantified the shape of NPLD troughs, using trough width, depth, wall slope and relief, from ~3000 profiles. We find that trough shape is variable within a single trough, between neighboring troughs, and between regions, and that trough morphology is overall not statistically different between the regions identified by Smith and Holt (2015). Roughly 88% of the trough cross-sections we investigated showed trough relief asymmetry and trough-parallel clouds were often observed near these asymmetrical troughs (per Smith et al., 2013). The remaining troughs were v-shaped and may be surface expressions of the v-shaped reflectors observed in SHARAD data (Smith & Holt, 2015). The mechanism for how these v-shaped cross-sections form is outside the scope of this study, but it is possible that regions of the NPLD sometimes experience erosional cyclic steps (that have no ice deposition post-hydraulic jump), leading to the high-side of trough walls decreased in relief over time. Our work can inform modeling studies similar to those of Bramson et al. (2019) that look at trough migration using representative trough morphologies, as well as comparisons between trough morphology recorded in the stratigraphy with modern-day troughs. Future work will aim to investigate how varying amounts of water/ice entrainment (i.e., changes in sediment supply) affect trough wall morphology over time under critical flow conditions.

Acknowledgments

This research was conducted at Dartmouth College and supported by a NASA Mars Data Analysis Grant (#80NSSC21K1097), a Dartmouth Scholarly Innovation and Advancement Award, and a National Science Foundation GRFP to K. Lutz (#2236868). We greatly appreciate the comments and suggestions provided by our reviewers.

Open Research

All imagery used in this manuscript is freely available for download through the Planetary Data System (PDS) Cartography and Imaging Sciences Node and the Caltech Murray Lab. The THEMIS VIS dataset (Christensen, 2002) was used for cloud identification and classification. Cross-sectional trough profiles were extracted used a HRSC and MOLA Blended 200m DEM (v2) (Fergason et al., 2018) resampled to 1000m/pixel. Figures were made with Matlab version R2021b (available under a Mathworks license at mathworks.com) and Python3 scripts published on GitHub (Lutz, 2023). Maps were made using ArcPro version 3.0.2 available under an Esri license (available at esri.com). The cloud atlas, topographic profiles, and derived metrics used to determine trough morphology across the NPLD are available at Figshare (Palucis et al., 2023) with a CC by 4.0 license.

References

Bramson, A. M., Byrne, S., Bapst, J., Smith, I. B., & McClintock, T. (2019). A Migration Model for the Polar Spiral Troughs of Mars. *Journal of Geophysical Research-Planets*, *124*(4), 1020–1043. https://doi.org/10.1029/2018JE005806

Christensen, P. R. (2002), ODYSSEY THEMIS VIS EDR V1.0 [Data set]. NASA Planetary Data System. https://doi.org/10.17189/1520344

Christensen, P. R., Jakosky, B.M., Kieffer, H.H, et al. (2004), The Thermal Emission Imaging System (THEMIS) for the Mars 2001 Odyssey Mission, *Space Science. Reviews, 110*, 85–130, https://doi.org/10.1023/B:SPAC.0000021008.16305.94

Cutts, J. (1973). Nature and Origin of Layered Deposits of Martian Polar Regions. *Journal of Geophysical Research*, *78*(20), 4231–4249. https://doi.org/10.1029/JB078i020p04231

Cutts, J., & Lewis, B. (1982). Models of Climate Cycles Recorded in Martian Polar Layered Deposits. *Icarus*, *50*(2–3), 216–244. https://doi.org/10.1016/0019-1035(82)90124-5

Diniega, S., & Smith, I. B. (2020). High-priority science questions identified at the Mars Workshop on Amazonian and Present-Day Climate. *Planetary and Space Science*, *182*, 104813. https://doi.org/10.1016/j.pss.2019.104813

Emmett, J., Murphy, J., & Kahre, M. (2020). Obliquity dependence of the formation of the Martian polar layered deposits. *Planetary and Space Science*, *193*, 105047. https://doi.org/10.1016/j.pss.2020.105047

Fergason, R. L., Hare, T. M., & Laura, J. (2018). HRSC and MOLA Blended Digital Elevation Model at 200m v2. Astrogeology PDS Annex, U.S. Geological Survey. http://bit.ly/HRSC_MOLA_Blend_v0

Fishbaugh, K. E., Byrne, S., Herkenhoff, K. E., Kirk, R. L., Fortezzo, C., Russell, P. S., & McEwen, A. (2010). Evaluating the meaning of “layer” in the martian north polar layered deposits and the impact on the climate connection. *Icarus*, *205*(1), 269–282. https://doi.org/10.1016/j.icarus.2009.04.011

Herkenhoff, K. E., & Plaut, J. J. (2000). Surface ages and resurfacing rates of the polar layered deposits on Mars. *Icarus*, *144*(2), 243–253. https://doi.org/10.1006/icar.1999.6287

Herny, C., Massé, M., Bourgeois, O., Carpy, S., Le Mouélic, S., Appéré, T., Smith, I.B., Spiga, A., Rodriguez, S. (2014). Sedimentation waves on the Martian North Polar Cap: Analogy with megadunes in Antarctica. *Earth and Planetary Science Letters, 403*, 56–66. https://doi.org/10.1016/j.epsl.2014.06.033

Howard, A., Cutts, J., & Blasius, K. (1982). Stratigraphic Relationships Within Martian Polar-Cap Deposits. *Icarus*, *50*(2–3), 161–215. https://doi.org/10.1016/0019-1035(82)90123-3

Howard, A. D. (2000). The role of eolian processes in forming surface features of the Martian polar layered deposits. *Icarus*, *144*(2), 267–288. https://doi.org/10.1006/icar.1999.6305

Hvidberg, C. S., Fishbaugh, K. E., Winstrup, M., Svensson, A., Byrne, S., & Herkenhoff, K. E. (2012). Reading the climate record of the martian polar layered deposits. *Icarus*, *221*(1), 405–419. https://doi.org/10.1016/j.icarus.2012.08.009

Khayat, A. S. J., Smith, M. D., & Guzewich, S. D. (2020). Detections of water vapor increase over the north polar troughs on Mars as observed by CRISM. *Geophysical Research Letters*, 47, e2019GL086195. https://doi.org/10.1029/2019GL086195

Kostic, S., & Parker, G. (2006). The response of turbidity currents to a canyon–fan transition: internal hydraulic jumps and depositional signatures. *Journal of Hydraulic Research, 44*(5), 631-653, https://doi.org/10.1080/00221686.2006.9521713

Koutnik, M.R., Byrne, S., Murray, B.C., Toigo, A.D., Crawford, Z.A. (2005). Eolian controlled modification of the Martian south polar layered deposits. *Icarus, 174*, 490–501. https://doi.org/10.1016/j.icarus.2004.09.015

Kruskal, W. H. & Wallis, W. A. (1952). Use of Ranks in One-Criterion Variance Analysis. *Journal of the American Statistical Association*, 47:260, 583-621, https://doi.org/10.1080/01621459.1952.10483441

Laskar, J., Levrard, B., & Mustard, J. F. (2002). Orbital forcing of the martian polar layered deposits. *Nature*, *419*(6905), 375–377. https://doi.org/10.1038/nature01066

Laskar, J., Correia, A. C. M., Gastineau, M., Joutel, F., Levrard, B., & Robutel, P. (2004). Long term evolution and chaotic diffusion of the insolation quantities of Mars. *Icarus*, *170*(2), 343–364. https://doi.org/10.1016/j.icarus.2004.04.005

Levrard, B., Forget, F., Montmessin, F., & Laskar, J. (2007). Recent formation and evolution of northern Martian polar layered deposits as inferred from a Global Climate Model. *Journal of Geophysical Research-Planets*, *112*(E6), E06012. https://doi.org/10.1029/2006JE002772

Lied, N. T. (1964). Stationary hydraulic jumps in a katabatic flow near Davis, Antarctica, 1961. *Aust. Meteor. Mag*, *47*, 40–51.

Lutz, K. A. (2023). NPLD Trough Profile Plotting and Metric Value Calculation (Version 1.0) [Software]. Zendo. https://doi.org/10.5281/zenodo.8157448

Malin, M. C., and Edgett, K. S. (2001), Mars Global Surveyor Mars Orbiter Camera: Interplanetary cruise through primary mission. *Journal of Geophysical Research-Planets*, *106*(E10), 23429– 23570, https://doi.org/10.1029/2000JE001455

Mann, H. B., & Whitney, D.R. (1947). On a Test of Whether one of Two Random Variables is Stochastically Larger than the Other. *Ann. Math. Statist. 18* (1) 50 - 60. https://doi.org/10.1214/aoms/1177730491

Palucis, M., Lutz, K. A., & Hawley, R. L. (2023). Data produced in Lutz et al. (2023): Investigating the Linkage Between Spiral Trough Morphology and Cloud Coverage on the Martian North Polar Layered Deposits [Data set]. figshare. https://doi.org/10.6084/M9.FIGSHARE.23692725

Parker, G., & Izumi, N. (2000). Purely erosional cyclic and solitary steps created by flow over a cohesive bed. *Journal of Fluid Mechanics, 419*, 203-238. https://doi.org/10.1017/S0022112000001403

Pathare, A. V., & Paige, D. A. (2005). The effects of martian orbital variations upon the sublimation and relaxation of north polar troughs and scarps. *Icarus*, *174*(2), 419–443. https://doi.org/10.1016/j.icarus.2004.10.030

Pettre, P., & Andre, J. (1991). Surface-Pressure Change Through Loewe Phenomena and Katabatic Flow Jumps - Study of 2 Cases in Adelie Land, Antarctica. *Journal of the Atmospheric Sciences*, *48*(4), 557–571. https://doi.org/10.1175/1520-0469(1991)048<0557:SPCTLP>2.0.CO;2

Rodriguez, J. A. P. & Tanaka, K. L. (2011). *Evidence for in-situ trough erosion in Planum Boreum, Mars*. Paper presented at the Fifth International Conference on Mars Polar Science and Exploration, Fairbanks, Alaska. 1323, Abstract 6015.

Rodriguez, J. A. P., Tanaka, K. L., Bramson, A. M., Leonard, G. J., Baker, V. R., & Zarroca, M. (2021). North polar trough formation due to in-situ erosion as a source of young ice in mid-latitudinal mantles on Mars. *Scientific Reports*, *11*(1), 6750. https://doi.org/10.1038/s41598-021-83329-3

Smith, I. B., & Holt, J. W. (2010). Onset and migration of spiral troughs on Mars revealed by orbital radar. *Nature*, *465*(7297), 450–453. https://doi.org/10.1038/nature09049

Smith, I. B., & Holt, J. W. (2015). Spiral trough diversity on the north pole of Mars, as seen by Shallow Radar (SHARAD). *Journal of Geophysical Research-Planets*, *120*(3), 362–387. https://doi.org/10.1002/2014JE004720

Smith, I.B., & Spiga, A. (2018). Seasonal variability in winds in the north polar region of Mars. *Icarus, 308*, 188–196. https://doi.org/10.1016/j.icarus.2017.10.005.

Smith, I. B., Diniega, S., Beaty, D. W., Thorsteinssan, T., Becerra, P., Bramson, A. M., et al. (2018). 6th international conference on Mars polar science and exploration: Conference summary and five top questions. *Icarus*, *308*, 2–14. https://doi.org/10.1016/j.icarus.2017.06.027

Smith, I. B., Hayne, P. O., Byrne, S., Becerra, P., Kahre, M., Calvin, W., et al. (2020). The Holy Grail: A road map for unlocking the climate record stored within Mars' polar layered deposits. *Planetary and Space Science*, *184*, 104841. https://doi.org/10.1016/j.pss.2020.104841

Smith, I. B., Holt, J. W., Spiga, A., Howard, A. D., & Parker, G. (2013). The spiral troughs of Mars as cyclic steps. *Journal of Geophysical Research-Planets*, *118*(9), 1835–1857. https://doi.org/10.1002/jgre.20142

Smith, I.B., Spiga, A., & Holt, J.W. (2015). Aeolian processes as drivers of landform evolution at the south pole of Mars. In *Geomorphology, Planetary Geomorphology: Proceedings of the 45th Annual Binghamton Geomorphology Symposium, held 12-14 September 2014 in Knoxville, Tennessee, USA*. (Vol. 240, pp. 54–69). https://doi.org/ 10.1016/j.geomorph.2014.08.026.

Taki, K., & Parker, G. (2005). Transportational cyclic steps created by flow over an erodible bed. Part 1. Experiments, *Journal of Hydraulic Research, 43*(5), 488-501, https://doi.org/10.1080/00221680509500147

Tanaka, K. L., Rodriguez, J. A. P., Skinner, J. A., Bourke, M. C., Fortezzo, C. M., Herkenhoff, K. E., et al. (2008). North polar region of Mars: Advances in stratigraphy, structure, and erosional modification. *Icarus*, *196*(2), 318–358. https://doi.org/10.1016/j.icarus.2008.01.021